ACS APPLIED MATERIALS & INTERFACES

Research Article

www.acsami.org

Vertical Convective Coassembly of Refractory YSZ Inverse Opals from Crystalline Nanoparticles

Roman Kubrin,*[,†] Jefferson J. do Rosario,[†] Hooi Sing Lee,[‡] Sweety Mohanty,[†] Raman P. Subrahmanyam,[§] Irina Smirnova,[§] Alexey Petrov,[⊥] Alexander Yu. Petrov,[‡] Manfred Eich,[‡] and Gerold A. Schneider[†]

[†]Institute of Advanced Ceramics, Hamburg University of Technology, Denickestrasse 15, 21073 Hamburg, Germany

[‡]Institute of Optical and Electronic Materials, Hamburg University of Technology, Eissendorfer Strasse 38, 21073 Hamburg, Germany

[§]Institute of Thermal Separation Processes, Hamburg University of Technology, Eissendorfer Strasse 38, 21073 Hamburg, Germany

[⊥]Institute of Physical Chemistry, University of Hamburg, Grindelallee 117, 20146 Hamburg, Germany

ABSTRACT: A facile deposition method of 3D photonic crystals made of yttrium-stabilized zirconia (YSZ) was developed. YSZ nanoparticles with primary particle size below 10 nm and cubic crystalline phase were synthesized by hydrothermal treatment of solutions of zirconyl nitrate, yttrium nitrate and acetylacetone. Before coassembly with polystyrene (PS) microspheres, a dispersant Dolapix CE64 was added to the dialyzed sol of YSZ nanoparticles to render their surface negatively charged. Vertical convective coassembly resulted in 3D ordered YSZ/PS hybrid films, which were inverted at 500 °C in air to produce inverse opals. The linear shrinkage of the coatings was in the range 15−20%, below previously reported values for YSZ. The obtained coatings demonstrated pronounced photonic properties and retained their ordered structure after annealing at 1000 °C for 2 h. Increasing the filling fraction of crystalline nanoparticles in the templates should enable production of fully functional 3D photonic crystals for applications in high-temperature photonics.

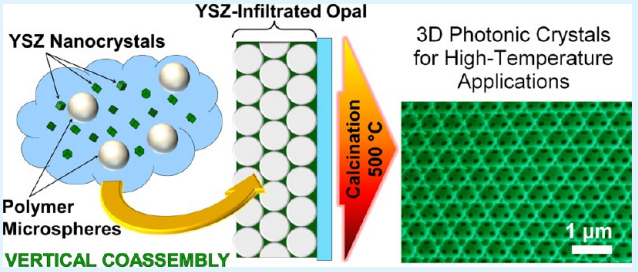

KEYWORDS: *vertical convective self-assembly, nanoparticle codeposition, high-temperature photonics, 3D photonic crystal, inverse opal, yttrium-stabilized zirconia*

INTRODUCTION

3D ordered macroporous (3DOM) ceramic coatings with the inverse opal morphology are attractive for various applications, such as wavelength-selective reflectors in sensitized solar cells,[1,2] because of their unique optical properties resulting from a periodic variation of the effective refractive index. Inverse opals made of titanium dioxide are the most popular realization of 3D photonic crystals because of the high refractive index of TiO_2 and a wide variety of applicable colloidal crystal templating processes, such as sol−gel infiltration,[3−8] atomic layer deposition,[9−11] nanoparticle infiltration,[12] and codeposition.[13−15] Inverse opals from other important ceramic materials, especially from those having more complex composition (e.g., solid solutions of mixed oxides)[16−19] or from nonoxides (carbides, nitrides),[20−22] are less studied and often much more difficult to produce.

Yttrium-stabilized zirconia (YSZ) is a material widely used for applications in which a combination of refractory properties, low thermal conductivity, high hardness, high thermal expansion coefficient, and high oxygen ion conductivity are demanded. There are several works employing YSZ inverse opals as the porous anode in solid-oxide fuel cells.[18,23−25] However, these only make use of the high porosity of inverse opal structure and do not involve their photonic functionality. Powdered samples of undoped zirconia inverse opals have also been studied.[26] A method to produce curvilinear photonic crystal stripes of ZrO_2 inverse opal has been developed.[27] Zirconia inverse opal films were used to obtain single-mode photonic lasing by infiltration with organic laser dyes.[28] Luminescent inverse opals made of zirconia doped with rare earth ions[29,30] or titanium[31] are also reported. To the best of our knowledge, synthesis of refractory YSZ inverse opal films of optical quality has not been demonstrated. This would constitute a major advance in the field of high-temperature photonics. Refractory photonic crystals could be used as next-generation thermal barrier coatings (TBC) that would not only inhibit heat transfer by thermal conduction but also reflect thermal radiation, whose contribution becomes more and more significant as the gas inlet temperature of a gas turbine increases.[32,33]

Inverse opals are usually obtained by a two-step deposition followed by inversion. In the first deposition step, an artificial direct opal template is produced by self-assembly of monodisperse particles of certain polymers or silica. In the

Received: September 24, 2013
Accepted: December 2, 2013
Published: December 9, 2013

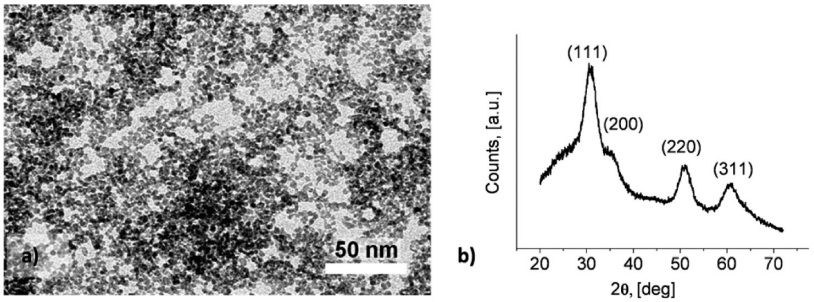

Figure 1. (a) TEM bright-field image and (b) XRD spectrum of the synthesized YSZ nanoparticles.

second step, this structure is infiltrated with a ceramic phase. Inversion of the direct structure is typically achieved by calcination of the polymer or selective etching of the silica template.

Established infiltration techniques are usually time-consuming and tedious. Furthermore, they all to a certain extent deal with the problem of inevitable volume change of the infiltrant between its initial chemical state (e.g., a solution of inorganic salts or alkoxides) and after accomplishment of the synthesis procedure (solid phase). The detrimental effect is magnified particularly when the material has to be exposed to high temperatures, under which crystallization, phase transformation(s), and densification of ceramics occur. These processes induce formation and broadening of cracks as well as coarsening of the pore structure.

As a measure for minimizing these negative effects of chemical transformation of the infiltrant, it was proposed to use dispersions of nanoparticles instead of conventional sol−gel precursors.[18] It was also suggested that the deposition of the sacrificial template and liquid-phase infiltration can be combined in a single process, referred to as codeposition or coassembly, where polymeric microspheres and ceramic precursors or nanoparticles are simultaneously deposited from mixed dispersions,[14,15,34−38] thus reducing the number of required processing steps and processing time.

Here we report on a facile all-colloidal, one-step codeposition method of YSZ refractory inverse opals. 3D photonic crystal films were grown from a dispersion containing sacrificial monodisperse polystyrene (PS) microspheres and crystalline YSZ nanoparticles obtained from hydrothermal synthesis. Initially positive surface charge of nanoparticles was reversed by adding an anionic dispersant in order to avoid heterocoagulation with PS particles. Spectra of reflectance of YSZ inverse opals featuring a pronounced photonic stopgap were measured for the first time. We also investigated the degradation of the structure at high temperatures.

MATERIALS AND METHODS

Preparation of the YSZ Nanocrystalline Sol. Crystalline nanoparticles of YSZ with primary particle size <10 nm were obtained following the procedure described by Guiot et al.[39] First, an aqueous solution of zyrconyl nitrate hydrate ($ZrO(NO_3)_2{\cdot}xH_2O$, 99%, Sigma-Aldrich) and yttrium nitrate hexahydrate ($Y(NO_3)_3{\cdot}6H_2O$, 99.9%, MaTecK GmbH, Jülich, Germany) was prepared. The concentration of Zr-ions was adjusted to 0.1 M and that of Y-ions to 0.05 M. Acetylacetone (puriss., Sigma-Aldrich) was then added to obtain a concentration of 0.1 M. The initially strongly acidic pH of the solution was changed to 7.0 by slowly adding 3 M aqueous solution of ammonia. Typically, 40 mL of freshly mixed precursor solution was sealed in a PTFE liner in an autoclave (High pressure reactor BR-25, Berghof GmbH, Eningen, Germany) and left for three days at 160 °C. Upon cooling to room temperature, a translucent stable sol of nanoparticles could be extracted. The sol was purified by dialysis in deionized water through a tubular cellulose membrane (Nadir, pore size 2.5−3 nm, Kalle GmbH, Wiesbaden, Germany) and then subjected to the ultrasonic treatment in order to break up agglomerates (Ultrasonic processor UP100H; Hielscher Ultrasonics). In this way, a transparent sol stable over at least several weeks was obtained. According to the authors of the method,[39] the concentration of yttria in the precipitated YSZ nanoparticles should be approximately 9 mol.%. In order to obtain the negative surface charge of the nanoparticles, a low molecular weight anionic organic dispersant Dolapix CE 64 (320 g/mol, Zschimmer & Schwarz Chemie GmbH, Lahnstein, Germany) was used.

Template Material and Preparation of the Substrates. Monodisperse PS particles with diameters of 500 nm (standard deviation = 9 nm) and 756 nm (standard deviation = 20 nm) were purchased from Microparticles GmbH (Berlin, Germany). Conventional soda-lime glass microscope slides (76 × 26 mm; Thermo Scientific) and quartz microscope slides (76 × 26 mm; Ted Pella, Inc., Redding, CA, USA), used as substrates, were cleaned by soaking in an alkaline detergent solution (Mucasol, Brand, Merz Hygiene GmbH, Frankfurt, Germany) for 2 h in an ultrasonic bath, brushing, rinsing subsequently in hot tap water and in deionized water, and blow drying by filtered nitrogen.

Co-assembly and Inversion of the Coatings. Typical vertical convective coassembly experiments were arranged as follows. Required volumes of stock dispersions of PS particles and YSZ nanoparticles (with addition of Dolapix) were diluted with deionized water to a desired concentration in a 50 mL Teflon beaker, homogenized by a magnetic stirrer, and filtered in order to remove large agglomerates and dust particles (Minisart NML, pore size 5 μm, Sartorius Stedim Biotech S.A.). The concentration of PS microspheres was usually fixed at 1 mg/mL and the concentration of nanoparticles was varied between 0.5 and 1 mg/mL. Beakers were put into a humidity chamber HCP 108 (Memmert GmbH, Schwabach, Germany) at constant temperature of 55 °C and relative humidity of 70−80%. One substrate was put into each beaker and left for several days until the desired length of the opaline film was achieved (20−30 mm). The inverse opals were obtained by calcination of the coassembled coatings in air at 500 °C for 30 min. The heating rate of 2 °C/min was used; the cooling rate was equal or lower. The same ramping rates were used in the annealing experiments in air. The dwell time at 1000 °C was 2 h.

Characterization. The morphology and size of the nanoparticles were studied by transmission electron microscopy (TEM, JEM-1101, JEOL). The zeta-potential of the dispersed nanoparticles was measured by Zetasizer 2000 (Malvern Instruments). The quality of the coassembled samples was investigated by scanning electron microscopy (SEM, Leo 1530 Gemini and Zeiss Supra 55 VP, Carl Zeiss Microscopy). The optical properties in the near-infrared spectral region were measured with a Fourier transform infrared spectrometer (FTIR, Bruker Tensor37, Bruker Optik) in the specular reflectance mode. The spectra in 0.8−1.7 μm wavelength range were collected using Halogen lamp, a CaF_2 beamsplitter, and an InGaAs detector. The recorded power spectrum of a mirrorlike reflected beam from the sample was normalized with the spectrum taken with an aluminum mirror. Reflectance spectra in the visible range were measured by a

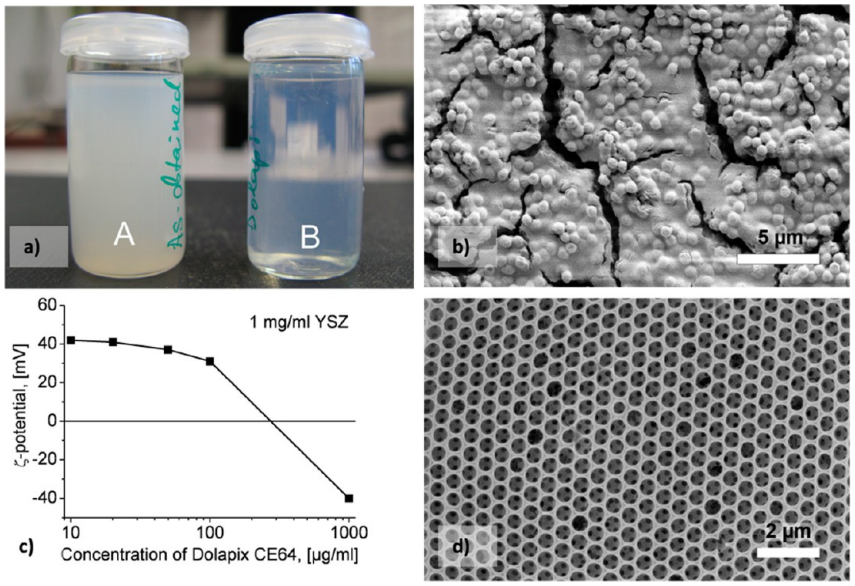

Figure 2. (a) Examples of the dispersion of YSZ nanoparticles (A) before and (B) after ultrasonic treatment; (b) typical morphology of the YSZ porous coatings deposited from dispersions of PS and YSZ without the dispersant (PS: 756 nm, 1 mg/mL, YSZ:2.5 mg/mL, no Dolapix); (c) Dependence of ζ-potential on the concentration of the dispersant; (d) YSZ inverse opal with dispersant (PS: 756 nm, 1 mg/mL, YSZ: 0.5 mg/mL, Dolapix: 0.5 mg/mL).

Perkin-Elmer UV−vis−NIR spectrometer Lambda 1050. X-ray diffraction (XRD)-patterns were obtained by a Bruker AXS D8 Advance diffractometer with Cu−Kα radiation and a GADDS detector.

RESULTS AND DISCUSSION

Synthesis of the Crystalline YSZ Nanoparticles. Hydrothermal synthesis of YSZ nanoparticles very closely followed the route described by Guiot et al.[39] For the chosen composition of the nitrate-based precursor solution, the value of pH was adjusted to 7 before the treatment in the autoclave. In agreement with the original work, any attempt to further increase the pH lead to fast condensation of solid particles. It was also observed that an excess of acetylacetone shifted the critical pH, where rapid condensation started, to lower values. After hydrothermal synthesis, the nanoparticle sol did not reach the state of full syneresis, but otherwise the products possessed all expected characteristics. Figure 1 shows that the formed nanoparticles had a primary particle size of less than 10 nm (Figure 1a) and were of crystalline structure (Figure 1b). The XRD spectrum corresponds to a cubic phase of YSZ (JCPDS 30−1468), which does not experience any phase transformations upon heating up to its melting point. In this way, the high-temperature stability of the produced macroporous structures should not suffer from the related abrupt density changes of the solid material.

The turbid appearance of the nanoparticle dispersion immediately after the synthesis pointed to the pronounced agglomeration because well-dispersed nanoparticles barely scatter light. The size of agglomerates could be successfully decreased by ultrasonication, as indicated by the sol turning transparent (Figure 2a).

Precluding Coagulation of the Binary YSZ/PS Dispersion. The value of pH in the mother liquor after dialysis and sonication was still acidic (4−5) and corresponding values of ζ-potential were in the range +40 to +45 mV. Positive surface charge of YSZ nanoparticles leads to a heterocoagulation of the dispersion once mixed with PS microspheres, which bear a permanent negative charge on the surface. The assembly of ordered hybrid PS/YSZ coatings would not be possible in this case (see Figure 2b). This problem would not occur for coassembly in SiO_2/PS[34] or SiO_2/PMMA system[14] because silica has the isoelectric point (IEP) in the range of low pH (<3)[40] and in aqueous media with neutral pH SiO_2 nanoparticles are always strongly negatively charged. The coassembly in the system TiO_2/PS was feasible only when pH was kept above 7 so that titania nanoparticles acquired sufficient negative charge.[15] The IEP of YSZ is usually about the pH of 7[40,41] and strong basic solutions should be necessary to obtain stable binary YSZ/PS dispersions. We attempted adjusting the pH with KOH up to about 12 but still observed rapid flocculation of the colloids. Further increase of pH was impractical because it would lead to excessive ionic strength of the liquid, which also promotes flocculation, and considerably etch glass substrates during the coassembly.

Organic dispersants are widely utilized in colloidal processing of ceramics.[42,43] Ammonium polyacrylates and particularly Dolapix CE 64 are often used for preparation of concentrated YSZ slips.[44−47] However, no data were available on application of Dolapix for diluted dispersions of YSZ powders, so the concentration of the deflocculant had to be optimized before starting the coassembly experiments. The results are presented in Figure 2c. The increase of the Dolapix concentration caused a reduction of the positive ζ-potential followed by a reversal of the surface charge and an increase in negative values. Sufficient electrostatic stabilization was established again when the concentration of the dispersant reached the order of 1 mg/mL, approximately equal to the nanoparticle load. The pH of the dispersion changed to 8.5. In the following experiments, a stock dispersion containing Dolapix with the concentration fixed equal to that of YSZ nanoparticles was used for dilution and mixing with PS microspheres. In this way, concentration of the dispersant varied within a range 0.5−1 mg/mL and was always sufficiently high to ensure stability of binary dispersions.

The negative charge on the surface of YSZ nanoparticles precluded heterocoagulation so that the coassembly of ordered

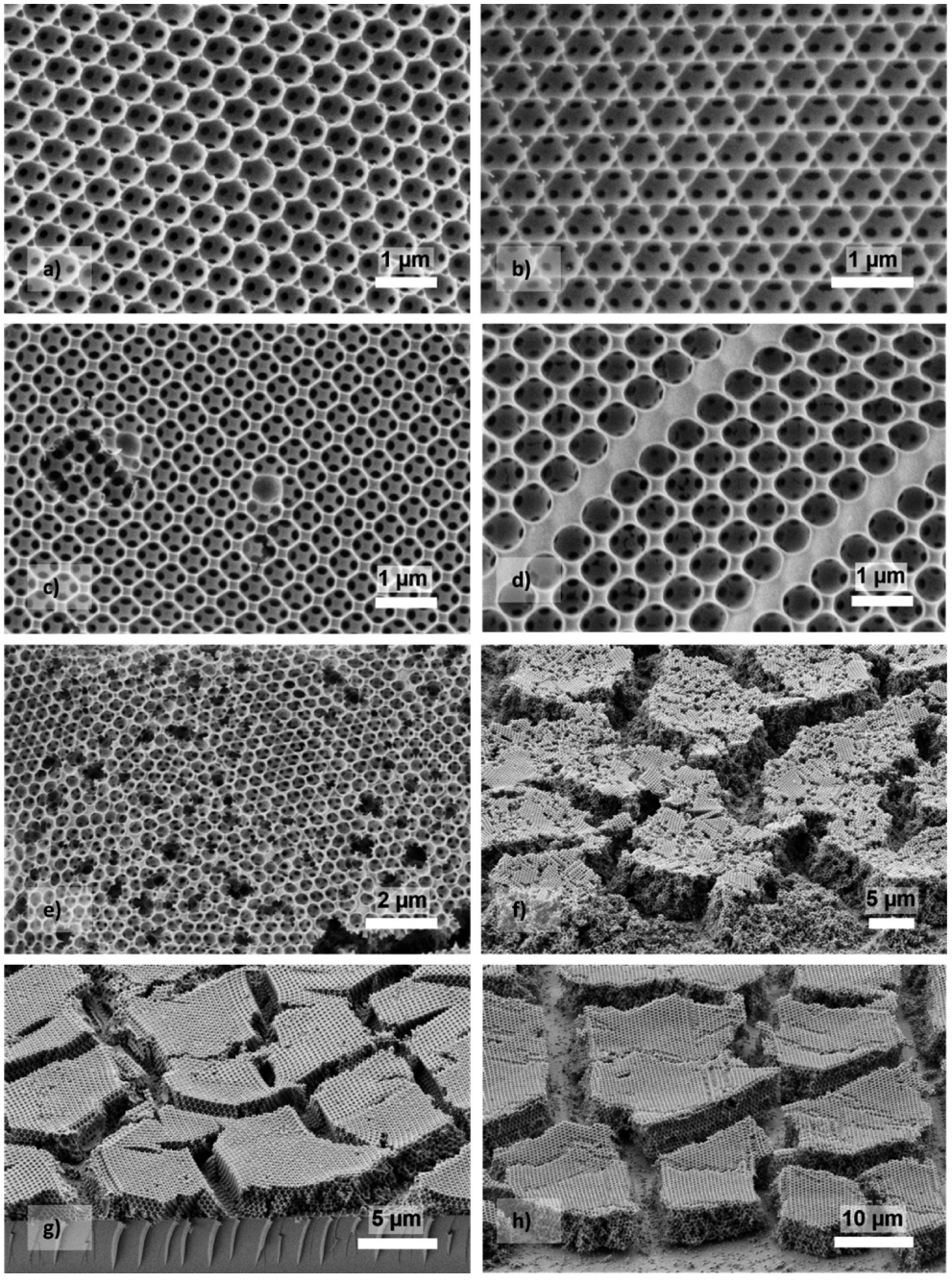

Figure 3. (a, b) Different ordered surface structures in the same sample (PS: 756 nm, 1 mg/mL, YSZ:1 mg/mL); (c) (110) crystallographic plane on the surface of codeposited YSZ inverse opal (PS: 500 nm, 1 mg/mL, YSZ:0.5 mg/mL); (d) (110) crystallographic plane on the surface of codeposited YSZ inverse opal (PS: 756 nm, 1 mg/mL, YSZ:0.5 mg/mL); (e) and (f) disordered structures in the non-iridescent area of the sample (PS: 500 nm, 1 mg/mL, YSZ:0.5 mg/mL); (g) cracks in the coating deposited with 1 mg/mL PS particles of 500 nm, and 0.5 mg/ml YSZ; (h) cracks in the coating deposited with 1 mg/mL PS particles of 756 nm and 0.5 mg/mL YSZ.

composite coatings became feasible (Figure 2d) and pronounced iridescence could be observed in the samples before and after calcination. The deposition rate could be varied between 5 to 8 mm/day by changing the relative humidity in the oven from 80 to 70% r.h., respectively. The temperature was kept constant at 55 °C.

Morphology of the YSZ Inverse Opal Films. By visual observation, the uniformity of deposition was worse than that of the PS artificial opals self-assembled without the ceramic nanoparticles and the dispersant. White noniridescent areas were observed in the samples, which usually designates lacking order in the porous structure. The inverse opal coatings deposited from the dispersions with lower concentration of nanoparticles (0.5 mg/mL) were more homogeneous and iridescent. The theoretical weight ratio of polystyrene and YSZ in a fully infiltrated opaline template is approximately 1:2 (PS:YSZ, corresponding to the volume ratio of 0.74:0.26). If the ratio of the components would not change upon deposition onto the substrate, the infiltration fraction of only 25% of the volume available for infiltration in the FCC lattice could be expected from the concentration ratio of 1 mg/mL:0.5 mg/mL (PS:YSZ) for the samples of the best quality. However, the

gravimetric investigation showed that the fraction of YSZ nanoparticles in the deposits (the only constituent left in the structure after the calcination) did not linearly scale with their concentration in the dispersion. There was no significant difference in the filling fraction of YSZ deposited from suspensions containing 0.8 and 1.0 mg/mL (in both cases, ceramic phases comprised 27 wt % of the total coating density). For the initial nanoparticle concentration of 0.5 mg/mL, their filling fraction was only slightly lower (21 wt %).

Morphology of the samples obtained with the PS particles of different sizes and different concentrations of YSZ nanoparticles is compiled in Figure 3. In the coassembled samples, domains with unusual (110) crystallographic orientation of the opaline FCC lattice were sometimes encountered (Figure 3c, d). One can also see disordered spots (Figure 3e, f). The latter ones appear in the noniridescent areas. These defects could probably be caused by the presence of substantial amounts of Dolapix acting as a surfactant and affecting the surface tension of water, the shape of the meniscus, and mechanics of the interaction of PS particles. Lack of ordering could be related to the local deviations of the volume ratio of microspheres and nanoparticles, with the concentration of the latter exceeding a certain optimal value.[48] We also observed inferior ordering in PS opals grown from a suspension containing the usual concentration of Dolapix without nanoparticles.

At the end of the sample, i.e., at a location where the coassembly process was interrupted, a thin stripe (a few millimeters along the growth direction) of the PS opal practically not infiltrated by the nanoparticles was sometimes observed. After the calcination, there were hardly any residues in such areas representing the zone of progressing cooperative self-assembly,[49] where PS particles already nucleated the opal layer but its infiltration with nanoparticles could not follow.

All produced samples were covered with a dense network of cracks, which gained considerable width upon calcination (Figure 3g, h). Pronounced cracking should be attributed to the shrinkage of the porous material. It is unlikely that the sintering processes could take place at the calcination temperature (500 °C) in a refractory material such as YSZ, even as a nanopowder. The width of the peaks in the XRD-spectra did not much change after the calcination (comparing Figure 4a, 4b) so that

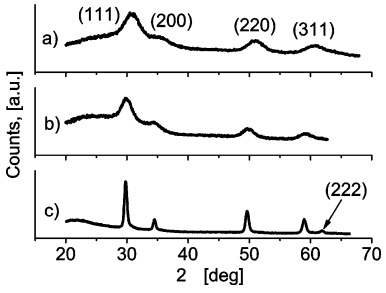

Figure 4. XRD spectra of (a) dried YSZ dispersion (repeated from Figure 1b); (b) YSZ inverse opal coatings after calcination at 500 °C; and (c) YSZ inverse opal coatings after sintering at 1000 °C.

the size of primary nanoparticles should not have significantly increased. Therefore, the volume change should be mostly due to drying (during the coassembly) and removal of the organic template and the dispersant (during the inversion of the structure).

Photonic Properties of the Deposited Coatings. Despite excessive cracking, the YSZ inverse opal coatings had a well-defined photonic response. As shown in Figure 5a, the samples deposited with the PS microspheres of 500 nm

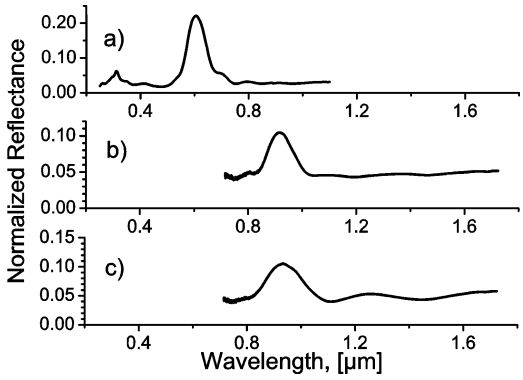

Figure 5. Reflectance spectra of the YSZ inverse opals: (a) deposited with PS particles of 500 nm and 0.5 mg/mL of YSZ; (b) PS particles of 756 nm and 0.5 mg/mL YSZ; and (c) PS particles of 756 nm and 1.0 mg/mL YSZ. Concentration of PS was 1 mg/mL in all cases.

featured a reflectance peak around wavelengths of 600 nm. The reflectance peak for the samples produced with 756-nm PS particles shifted to 900−950 nm (Figure 5b). This peak corresponds to the stopgap in ΓL-direction of the so-obtained 3D photonic crystal.[33] It was observed at the same wavelength for the samples deposited from dispersions of 0.5 and 1.0 mg/mL YSZ (comparing Figure 5b and 5c). This confirms that the concentration of nanoparticles in the dispersion does not strongly affect their filling fraction in the PS template.

When compared with TiO_2 inverse opals produced by conventional self-assembly and atomic layer deposition,[10,11] the stopgaps of YSZ photonic crystals are substantially blue-shifted. For example, for the inverse opals from titania with the anatase structure and the initial pore size of 756 nm the reflectance peak was located between 1400 and 1500 nm. Such a shift cannot be simply explained by the difference of refractive indices of TiO_2 (2.4[11]) and YSZ (2.1[50]) and should be related to the low initial filling fraction of YSZ and the decrease of the periodicity constant of the photonic crystal due to the shrinkage. From the SEM, the final pore size of the coatings obtained with 500 nm PS particles was approximately 430 nm. For the PS particles of 756 nm, the final pore size was about 600 nm. We obtained a figure of 15−20% lateral shrinkage. This is less than that observed for zirconia inverse opals produced by sol−gel methods[18,24−26] but still too much for any practical application of the photonic coatings because a considerable fraction of incident light would be either diffusely scattered on structure irregularities caused by the cracks or even penetrate through the cracks unaffected by the photonic crystal. For the application in TBCs, several photonic crystal films with different periodicity constants should be stacked upon each other,[10,33] so that the cracks can be filled with the subsequent layers of the inverse opals. In fact, certain crack density is also required in order to ensure the strain tolerance of the TBCs during the thermal cycling.[51] For applications that do not rely on multilayer coatings, a means to preclude or minimize cracking should be developed.

To decrease the extent of shrinkage, the deposition procedure should be modified as to allow denser packing of nanoparticles. The main obstacle for improvement in our method is the necessity of large amounts of the dispersant. Assuming that the ratio of YSZ and Dolapix does not

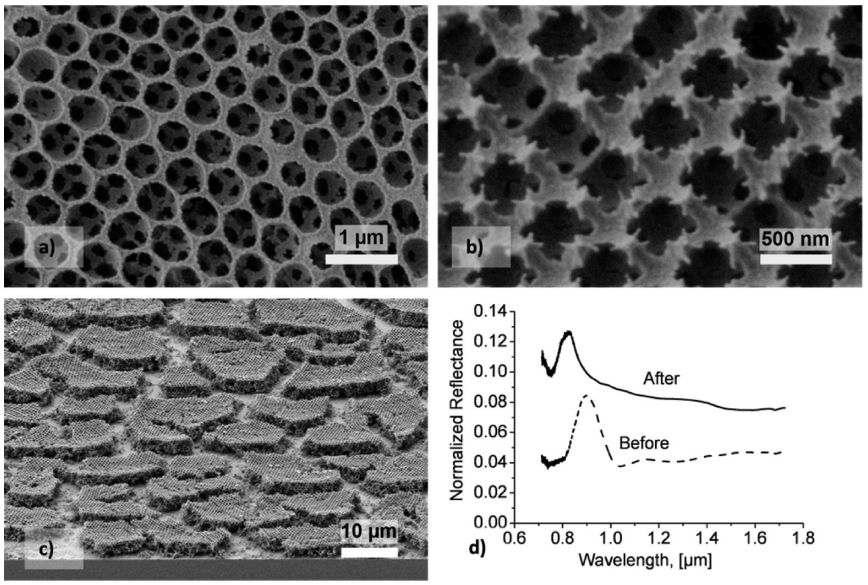

Figure 6. Morphology of the coatings sintered at 1000 °C: (a) made from PS particles of 756 nm and 0.5 mg/mL YSZ; (b, c) made from PS particles of 756 nm and 1 mg/mL YSZ; and (d) reflectance spectra of the YSZ inverse opal before and after sintering.

dramatically change in the meniscus where the self-assembly takes place and taking into account the theoretical density of cubic YSZ of 5.96 g/cm^3 (JCPDS 30−1468), the density of Dolapix CE 64 of 1.2 g/cm^3 and the amount of active matter of about 65%,[52] then the 1:1 weight ratio used in our experiments corresponds to the volume ratio of 1:2.9 (YSZ:Dolapix). This implies an approximately 75% volume decrease upon calcination as the worst case scenario. Even if the actual amount of the dispersant in the deposited layer is substantially lower, it still should be considered as the main optimization parameter of the proposed vertical coassembly method. Ideally, the use of dispersants should be completely avoided. An alternative approach would be to change the surface charge of the microspheres (using cationic polymer particles for the opaline templates) rather than attempting to change the charge on the nanoparticles. This modification of the coassembly technique is currently being investigated.

High-Temperature Stability of YSZ 3D Photonic Crystals. As the final experimental step in the present work, the stability of the porous structure of YSZ films at high temperatures was studied. The changes in morphology of the coatings and optical properties are presented in Figure 6. First, one can see that the shape of pores mostly stays intact and that the photonic properties are maintained. Inverse opals made of titanium dioxide usually undergo anatase-to-rutile phase transformation below 1000 °C, which provokes fast degradation of the pore structure.[53] As opposed to TiO_2, YSZ is a classical refractory material so that it is expected to have a superior stability. Our results support the previous study on sol−gel-templated YSZ inverse opals,[18] including the first signs of a noticeable grain growth starting at the temperatures around 1000 °C. The increase of crystallite size in our case is indicated in SEM by the appearance of a fine grainy structure in the pore walls (Figure 6a) and by the decrease in line width of the XRD spectra (Figure 4c). The size of large pores also changed; additional shrinkage was limited to below 5% of the initial size of PS particles, as assessed from SEM. The corresponding shift in the position of the photonic stopgap could be found in the spectra of reflectance (Figure 6d). According to Lashtabeg et al.,[18] at even higher temperatures, sintering processes in YSZ inverse opals are substantially accelerated. It can be anticipated that refractory inverse opals with excellent photonic properties and long-term stability in the temperature range up to 1000 °C could be produced by further elaboration of the proposed deposition method, if the filling fraction of YSZ in the opaline template could be further increased. For the temperatures exceeding this limit, other materials and/or special techniques for stabilization of pore structure will be required.

CONCLUSIONS

We have demonstrated a method for codeposition of refractory ceramic inverse opals, which combines self-assembly of the polystyrene opaline templates with their simultaneous infiltration by crystalline ceramic nanoparticles. Lateral shrinkage of the porous coating upon calcination (15−20%) was lower than that reported for sol−gel infiltrated zirconia inverse opals. Measurements of reflectance spectra of the YSZ 3D photonic crystals could be performed for the first time. The deposited coatings showed a good photonic response, which was, however, limited to below 25% of reflectance of the reference mirror by shrinkage-induced cracks. It can be expected that the use of anionic dispersing agents can be avoided by replacing plain polystyrene microspheres with cationic monodisperse polymer particles. This would allow further decreasing the shrinkage caused by drying and calcination of the photonic crystal coatings so that their unique optical properties could be efficiently utilized in the field of high-temperature photonics. The long-term stability of the YSZ inverse opals for temperatures up to 1000 °C potentially could be achieved by increasing the packing density of nanoparticles during the coassembly.

AUTHOR INFORMATION

Corresponding Author

*E-mail: roman.kubrin@tuhh.de.

Notes

The authors declare no competing financial interest.

■ ACKNOWLEDGMENTS

Financial support from the Hamburg Ministry of Science and Research and the Joachim Herz Stiftung as a part of the Hamburg Initiative for Excellence in Research (LEXI) and the German Research Foundation (DFG) via Collaborative Research Center SFB 986 "Tailor-Made Multi-Scale Materials Systems: M^3" (projects C2, C4, C5, and C6) is gratefully acknowledged. The authors thank Dr. Robert Pasquarelli for fruitful discussions and comments on the manuscript.

■ ABBREVIATIONS

YSZ, yttrium-stabilized zirconia
PS, polystyrene
3DOM, 3D ordered macroporous (material)
TBC, thermal barrier coatings
PTFE, polytetrafluoroethylene
IEP, isoelectric point
FCC, face-centered cubic (lattice)

■ REFERENCES

(1) Mihi, A.; Calvo, M.; Anta, J.; Miguez, H. *J. Phys. Chem. C* **2008**, *112*, 13−17.
(2) Toyoda, T.; Shen, Q. *J. Phys. Chem. Lett.* **2012**, *3*, 1885−1893.
(3) Holland, B. T.; Blanford, C. F.; Stein, A. *Science* **1998**, *281*, 538−540.
(4) Wijnhoven, J. E. G. J.; Vos, W. L. *Science* **1998**, *281*, 802−804.
(5) Kuai, S. L.; Hu, X. F.; Truong, V.-V. *J. Cryst. Growth* **2003**, *259*, 404−410.
(6) Dong, W.; Marlow, F. *Microporous Mesoporous Mater.* **2007**, *99*, 236−243.
(7) Galusha, J. W.; Tsung, C. K.; Stucky, G. D.; Bartl, M. H. *Chem. Mater.* **2008**, *20*, 4925−4930.
(8) Li, Y.; Piret, F.; Léonard, T.; Su, B.-L. *J. Colloid Interface Sci.* **2010**, *348*, 43−48.
(9) King, J. S.; Graugnard, E.; Summers, C. J. *Adv. Mater.* **2005**, *17*, 1010−1013.
(10) Kubrin, R.; Lee, H. S.; Zierold, R.; Yu. Petrov, A.; Janssen, R.; Nielsch, K.; Eich, M.; Schneider, G. A. *J. Am. Ceram. Soc.* **2012**, *95*, 2226−2235.
(11) Lee, H. S.; Kubrin, R.; Zierold, R.; Petrov, A. Y.; Nielsch, K.; Schneider, G. A.; Eich, M. *Opt. Mater. Express* **2013**, *3*, 1007−1019.
(12) Kwak, E. S.; Lee, W.; Park, N.-G.; Kim, J.; Lee, H. *Adv. Funct. Mater.* **2009**, *19*, 1093−1099.
(13) Ruani, G.; Ancora, C.; Corticelli, F.; Dionigi, C.; Rossi, C. *Sol. Energy Mater. Sol. Cells.* **2008**, *92*, 537−542.
(14) Hatton, B.; Mishchenko, L.; Davis, S.; Sandhage, K. H.; Aizenberg, J. *Proc. Natl. Acad. Sci. U.S.A.* **2010**, *107*, 10354−10359.
(15) Seo, Y. G.; Woo, K.; Kim, J.; Lee, H.; Lee, W. *Adv. Funct. Mater.* **2011**, *21*, 3094−3103.
(16) Shim, J. H.; Chao, C. C.; Huang, H.; Prinz, F. B. *Chem. Mater.* **2007**, *19*, 3850−3854.
(17) Li, H.; Zhang, L.; Dai, H.; He, H. *Inorg. Chem.* **2009**, *48*, 4421−4434.
(18) Lashtabeg, A.; Drennan, J.; Knibbe, R.; Bradley, J. L.; Lu, G. Q. *Microporous Mesoporous Mater.* **2009**, *117*, 395−401.
(19) Rudisill, S. G.; Hein, N. M.; Terzic, D.; Stein, A. *Chem. Mater.* **2013**, *25*, 745−753.
(20) Rugge, A.; Park, J. S.; Gordon, R. G.; Tolbert, S. H. *J. Phys. Chem. B* **2005**, *109*, 3764−3771.
(21) Sung, I.-K.; Christian; Mitchell, M.; Kim, D.-P.; Kenis, P. J. A. *Adv. Funct. Mater.* **2005**, *15*, 1336−1342.
(22) Zhou, J.; Li, H.; Ye, L.; Liu, J.; Wang, J.; Zhao, T.; Jiang, L.; Song, Y. *J. Phys. Chem. C* **2010**, *114*, 22303−22308.
(23) Munakata, H.; Otani, M.; Kanamura, K. *J. Fuel Cell Sci. Technol.* **2008**, *5*, 031206.
(24) Zhao, J. P.; Li, Y.; Xin, W. H.; Li, X. *J. Solid State Chem.* **2008**, *181*, 239−244.
(25) An, Y.; Skinner, S. J.; McComb, D. W. *J. Mater. Chem.* **2010**, *20*, 248.
(26) Schroden, R. C.; Al-Daous, M.; Blanford, C. F.; Stein, A. *Chem. Mater.* **2002**, *14*, 3305−3315.
(27) Vekris, E.; Ozin, G. A.; Kitaev, V. *Adv. Mater.* **2006**, *18*, 2481−2485.
(28) Nishijima, Y.; Ueno, K.; Juodkazis, S.; Mizeikis, V.; Misawa, H.; Maeda, M.; Minaki, M. *Opt. Express* **2008**, *16*, 13676−13684.
(29) Qu, X.; Song, H.; Bai, X.; Pan, G.; Dong, B.; Zhao, H.; Wang, F.; Qin, R. *Inorg. Chem.* **2008**, *47*, 9654−9659.
(30) Qu, X.; Song, H.; Pan, G.; Bai, X.; Dong, B.; Zhao, H.; Dai, Q.; Zhang, H.; Qin, R.; Lu, S. *J. Phys. Chem. C* **2009**, *113*, 5906−5911.
(31) Cong, Y.; Liu, D.; Yu, N.; Yang, Q.; Niu, J. *Nanosci. Nanotechnol. Lett.* **2011**, *3*, 151−154.
(32) Shklover, V.; Braginsky, L.; Witz, G.; Mishrikey, M.; Hafner, C. *J. Comput. Theor. Nanosci.* **2008**, *5*, 862−893.
(33) Lee, H. S.; Kubrin, R.; Zierold, R.; Petrov, A. Y.; Nielsch, K.; Schneider, G. A.; Eich, M. *J. Opt. Soc. Am. B* **2012**, *29*, 450−457.
(34) Zhou, Q.; Dong, P.; Cheng, B. *J. Cryst. Growth* **2006**, *292*, 320−323.
(35) Wang, J.; Li, Q.; Knoll, W.; Jonas, U. *J. Am. Chem. Soc.* **2006**, *128*, 15606−15607.
(36) Doong, R.; Chang, S.; Hung, Y.; Kao, I. *Sep. Purif. Technol.* **2007**, *58*, 192−199.
(37) Wang, J.; Ahl, S.; Li, Q.; Kreiter, M.; Neumann, T.; Burkert, K.; Knoll, W.; Jonas, U. *J. Mater. Chem.* **2008**, *18*, 981−988.
(38) Zheng, Z.; Gao, K.; Luo, Y.; Li, D.; Meng, Q. B.; Wang, Y.; Zhang, D. *J. Am. Chem. Soc.* **2008**, *130*, 9785−9789.
(39) Guiot, C.; Grandjean, S.; Lemonnier, S.; Jolivet, J.-P.; Batail, P. *Cryst. Growth Des.* **2009**, *9*, 3548−3550.
(40) Kosmulski, M. *Surface charging and Points of Zero Charge*; CRC Press: Boca Raton, FL, 2009.
(41) Jia, Y.; Duran, C.; Hotta, Y.; Sato, K.; Watari, K. *J. Colloid Interface Sci.* **2005**, *291*, 292−295.
(42) Sigmund, W. M.; Bell, N. S.; Bergström, L. *J. Am. Ceram. Soc.* **2000**, *83*, 1557−1574.
(43) Lewis, J. A. *J. Am. Ceram. Soc.* **2000**, *83*, 2341−2359.
(44) González, S.; Ferrari, B.; Moreno, R.; Baudín, C. *J. Am. Ceram. Soc.* **2005**, *88*, 2645−2648.
(45) Albano, M. P.; Garrido, L. B. *Mater. Sci. Eng., A* **2006**, *420*, 171−178.
(46) Hasanuzzaman, M.; Rafferty, A.; Olabi, A. G.; Prescott, T. *Int. J. Nanomanuf.* **2007**, *1*, 524−536.
(47) Garcia, E.; Mesquita-Guimarães, J.; Miranzo, P.; Osendi, M. I.; Wang, Y.; Lima, R. S.; Moreau, C. *J. Therm. Spray Technol.* **2010**, *19*, 286−293.
(48) Kumnorkaew, P.; Weldon, A. L.; Gilchrist, J. F. *Langmuir* **2010**, *26*, 2401−2405.
(49) Yang, L.; Wang, J.; Zhang, Y.; Luo, Y.; Li, D.; Meng, Q. *Langmuir* **2012**, *28*, 4160−4167.
(50) Wood, D. L.; Nassau, K. *Appl. Opt.* **1982**, *21*, 2978−2981.
(51) Stöver, D.; Funke, C. *J. Mater. Process. Technol.* **1999**, *92*−*93*, 195−202.
(52) Rao, S. P.; Tripathy, S. S.; Raichur, A. M. *Colloids Surf., A* **2007**, *302*, 553−558.
(53) Wijnhoven, J. E. G. J.; Bechger, L.; Vos, W. L. *Chem. Mater.* **2001**, *13*, 4486−4499.